Chemistry and Physics of Lipids 201 (2016) 21–27

Contents lists available at ScienceDirect

Chemistry and Physics of Lipids

journal homepage: www.elsevier.com/locate/chemphyslip

Measurement of the bending elastic modulus in unilamellar vesicles membranes by fast field cycling NMR relaxometry

Gabriela A. Dominguez, Josefina Perlo[1], Carla C. Fraenza, Esteban Anoardo*

LaRTE—FaMAF, Universidad Nacional de Córdoba and IFEG—CONICET, Ciudad Universitaria, X2016LAE, Córdoba, Argentina

ARTICLE INFO

Article history:
Received 6 July 2016
Received in revised form 22 September 2016
Accepted 31 October 2016
Available online 2 November 2016

PACS:
06.60.Mr
76.60.-k
87.64.kj

Keywords:
Liposomes
Lipid dynamics
Bending modulus
NMR relaxometry

ABSTRACT

The elastic properties of lipid membranes can be conveniently characterized through the bending elastic modulus κ. Elasticity directly affects the deformability of a membrane, morphological and shape transitions, fusion, lipid-protein interactions, etc. It is also a critical property for the formulation of ultradeformable liposomes, and of interest for the design of theranostic liposomes for efficient drug delivery systems and/or different imaging contrast agents. Measurements of κ in liposome membranes have been made using the fast field cycling nuclear magnetic relaxometry technique. We analyze the capability of the technique to provide a consistent value of the measured quantity under certain limiting conditions. Relaxation dispersions were measured acquiring a minimal quantity of points, within a reduced Larmor frequency range and, under inferior experimental conditions (in the presence of magnetic field in-homogeneity and lower power supply stability). A simplified model is discussed, showing practical advantages when fitting the data within the reduced frequency range. Experiments are contrasted with standard measurements performed in a state-of-the-art relaxometer. The methodology was tested in samples of 1,2-dimyristoyl-*sn*-glycero-3-phosphocholine with different percentiles of cholesterol. We observe a tendency to a decrease in κ with increasing temperature, and a tendency to increase with the cholesterol percentile.

1. Introduction

Lipid vesicles can be used as idealized model systems of real biomembranes. They have attracted much interest in biophysical research, particularly for the study of different processes related to the viscoelastic and mechanical properties of the membrane. The bending elastic modulus, a quantity reflecting the amount of energy needed to modify the intrinsic curvature of a bilayer, determines important biological functions of cells, like cell fusion, lipid–protein interactions and lipid-mediated protein activity (Katsaras and Guberlet, 2000; Groves, 2007; Park et al., 2010; Mouritsen, 2004). The effects of sterols (particularly cholesterol) on the membrane flexibility was frequently characterized through the bending elastic modulus (Méléard et al., 1997; Henriksen et al., 2004). Ultra-deformable liposomes used as transdermal carriers are formulated to have critical elastic properties through the addition of selected additives (Cevc and Gebauer, 2003). Therefore, reliable and non-invasive methods to characterize the elastic properties of membranes are attractive for both fundamental research and industrial applications.

In the last years, lipids and membranes came back into scene, with a tremendous need for the understanding of many lipid-mediated processes (Mouritsen, 2004; Rheinstädter and Mouritsen, 2013). The presence of proteins locally affects the elastic properties of the membrane thereby affecting the fluctuation spectrum of it. This has a direct impact on the lipid-protein dynamics and influence protein–protein processes like amyloid aggregation (Kotler et al., 2014) and other processes with direct impact on the human health (Tomaiuolo, 2014; Pretorius et al., 2016; Lasalvia et al., 2016). From a different perspective, non-specific interactions between proteins and the bilayer as a physical entity (chacterized by certain mesoscopic properties like e.g. elasticity or thickness) regulate protein activity (Lundbæk et al., 2010; Soubias et al., 2010; Brown, 2012; Epand et al., 2015). Today, it is clear that a close relationship exist between the elastic properties of the membrane, and a myriad of processes involving both lipids and embebed proteins.

* Corresponding author.
E-mail address: anoardo@famaf.unc.edu.ar (E. Anoardo).
[1] Current address: Magritek GmbH, Aachen, Germany.

http://dx.doi.org/10.1016/j.chemphyslip.2016.10.006
0009-3084/

1,2-Dimyristoyl-*sn*-glycero-3-phosphocholine (DMPC)–cholesterol mixtures have been studied by different authors in the past, not only using different experimental techniques, but also with computational resources. Still, uncler features persist concerning how the cholesterol modulates the viscoelastic properties of a DMPC membrane, even with no consensus on the corresponding phase diagram (de Meyer et al., 2010). How cholesterol modulates the elastic behaviour of the membrane strongly depends upon the saturation of the hidrocarbon chains of the lipids. When lipids have fully saturated chains, like DMPC, cholesterol increases κ. However, it does not have mayor effects for monoinsaturated chains (Pan et al., 2008a). Depending on the concentration, part of the lipids in the membrane will be in a cholesterol-induced ordered state (Fraenza et al., 2014). However, such ordered lipids are not necessarily isolated, they may tend to aglomerate into domains (or "rafts") in coexistence with a more "fluid" phase (Rheinstädter and Mouritsen, 2013). Plenty of questions remain on the lipid dynamics and order, and the conextion between these and the mesoscopic behaviour of the membrane.

Different experimental techniques are available for the study of membrane elasticity (Dimova, 2014; Monzel and Sengupta, 2016). However, easily available techniques implemented through benchtop instruments (generally based on optical microscopy) are only useful for studies in giant unilamellar vesicles (GUV, micrometer scale). Examples of this sort are video microscopy analysis of contour fluctuations (Méléard et al., 1997; Henriksen et al., 2004; Duwe and Sackmann, 1990; Minetti et al., 2016) and fluorescence confocal microscopy (Tian et al., 2009). On the other hand, successful techniques used for the study of membrane elasticity in large unilamellar vesicles (LUV, between 100 nm and 1 μm) tend to be based on large scale instrumentation like conventional nuclear magnetic resonance (NMR) (Althoff et al., 2002; Kinnun et al., 2015) or neutron spin-echo (NSE) systems (Yi et al., 2009; Armstrong et al., 2014). It is worth mentioning atomic force microscopy (AFM) as an exception, allowing the study of mechanical properties in LUV with small scale instrumentation, although more invasive than the previous methods (Delmore and Fery, 2006; Takechi-Haraya et al., 2016). In contrast to optical based techniques, NMR and NSE can be extended to small unilamellar vesicles (SUV, less than 100 nm).

NMR Relaxation is a powerful technique for the study of molecular dynamics. At high resolution, local positions of the acyl chains can be analyzed independently (Trouard et al., 1999; Brown et al., 2002; Martinez et al., 2002). A unified analysis of the frequency and temperature-dependence of ^{13}C and ^{2}H relaxation in DMPC revealed that individual segmental or molecular reorientations alone deficiently explain the low-frequency behavior of the observed results. In contrast, three-dimensional collective fluctuations can be argued consistently for the account of spin-relaxation in a broad MHz frequency range (corresponding to external magnetic field strengths between 0.382 and 14.6T) (Nevzorov and Brown, 1997).

Fast field-cycling (FFC) NMR relaxometry is an NMR technique already used in a series of compounds ranging from solid to liquids, and a large variety of soft materials (Kimmich and Anoardo, 2004; Fujara et al., 2014). The technique belongs to the "time-domain" NMR, since fast-switchable magnets having poor homogeneity (in terms of spectral resolution) are used. Proton relaxation rates obtained from this method are mainly driven by fluctuations of the ^{1}H–^{1}H dipolar couplings. It has been successfully used for the study of multilamellar vesicles (MLV) (Kimmich et al., 1983; Rommel et al., 1988; Struppe et al., 1997), and recently applied for the study of lipid molecular dynamics (strongly related with the viscoelastic properties) in LUV (Fraenza et al., 2014; Meledandri et al., 2009; Perlo et al., 2011). In these studies no attempt was made to use the FFC technique to measure a particular physical parameter.

Although the present work is heavily based on the previous studies described in Refs. (Fraenza et al., 2014; Meledandri et al., 2009; Perlo et al., 2011), now we concentrate on the limiting experimental conditions and model simplifications that would allow a systematic measurement of κ. It will turn out that κ can be measured within a restricted frequency range, using a simplified physical model, from data obtained using a FFC machine having a magnet with a lower homogeneity and a lower magnetic field stability (compared to the current state-of-the-art).

This work was planned with the idea of evaluating the feasibility for a small compact benchtop low-power & low-cost instrument, aimed for the measurement of the bending elastic modulus (κ). To do this, we measured the proton spin-lattice relaxation rate $R_1(\nu)$ within a restricted Larmor frequency (ν) range (typically from 100 kHz to 2.5 MHz), but using a standard instrument with degraded magnet homogeneity (~350 ppm/cm^3), and a lower magnet-current stability (~1:10^4). The idea supporting this study concerns the potential use of small-sized air-core field-cycling electromagnets (Kruber et al., 2013, 2014, 2015), resulting in important advantages in the electric parameters at the expense of a lower spatial homogeneity of the magnetic field. This fact in turn favors a lower technical demand on the power supply stability. Since the R_1 relaxation dispersion can still be measured at lower resolution, the main limitation of this approach concerns the signal to noise ratio of the NMR signal.

Since the total experimental time is also an important factor, we also reduced the quantity of measured R_1 experimental points and the number of signal acquisitions used for each R_1 measurement. We show here that even under extreme unfavorable conditions (just a few points having large errors), it is possible to measure κ within an uncertainty of ±20%. It is important to mention that at normal FFC conditions (20 ppm magnet and current stability better than 1:10^5) this error can be hardly decreased to less than ±10%.

In order to test the sensitivity of the measurements to a change in κ, experiments were done in DMPC liposomes prepared with different cholesterol content, a well known regulator of the membrane elasticity. However, it should be emphasized that the novel feature of this manuscript does not rely in this point. The behavior of the membrane in terms of cholesterol content has been studied in a previous work (Fraenza et al., 2014) and it is outside the scope of the present study.

2. Relaxometric analysis

We find it convenient to introduce the relaxometric properties using information already available in the literature. Fig. 1 shows the spin-lattice relaxation rate dispersion of DMPC liposomes having a radius $R_0 = 54$ nm (no cholesterol content). Measurements were performed at a temperature of 310 K. Data and the corresponding model are extracted from Ref. (Meledandri et al., 2009). The relaxation rate dispersion of lipid protons can be explained (black solid line) in terms of the following dynamical processes:

1. Local order fluctuations due to shape fluctuations of the liposome spheroid (OF).
2. Translational diffusion of the lipid molecules on a curved surface (D).
3. Rotations of the lipid molecules (R).
4. Fast internal motions within the lipid molecules (F).

The black solid line curve $R_1(\boldsymbol{\nu})$ corresponding to the model (see Fig. 1) was obtained after adding the contributions of each

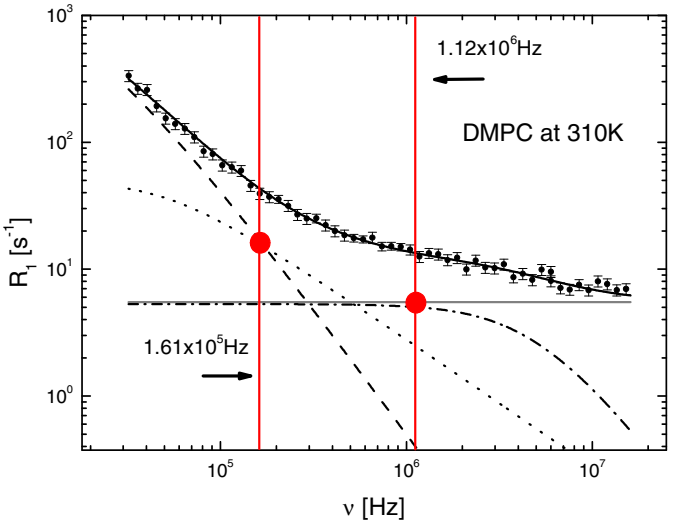

Fig. 1. Relaxation rate dispersion of DMPC liposomes of 54 nm radius at 310 K (data extracted from Ref. (Meledandri et al., 2009)) (For interpretation of the references to color in the text, the reader is referred to the web version of this article.).

mechanism:

$$R_1 = R_1^{OF} + R_1^D + R_1^R + R_1^F. \quad (1)$$

Details of the involved physical models are not part of the discussion of interest in this manuscript (the reader can refer to Ref. Meledandri et al., 2009 and references therein).

The two crossing points in Fig. 1 (in red) indicate particular frequencies where two important features can be observed:

1. The point on the left side defines the frequency (1.61×10^5Hz in the Figure) at which the relative contributions of translational diffusion and order fluctuations cross. That is, the minimum frequency ν_m from which order fluctuations start to be dominant over translational diffusion.
2. The point on the right side defines the frequency where the rotational diffusion contribution starts to be dispersive. That is, the maximum frequency ν_M up to which rotational diffusion cannot be distinguished from the rest of the fast isotropic-like motions.

Therefore, within the frequency range $\Delta\nu = \nu_M - \nu_m$, order fluctuations become the dominant dispersive relaxation contribution, and both fast motions and rotational diffusion can be replaced by a unique frequency-independent constant (offset), i.e., $R_1^{offset} = R_1^R + R_1^F$:

$$R_1(\nu) = R_1^{OF}(\nu) + R_1^D(\nu) + R_1^{offset}. \quad (2)$$

Eq. (2) represents a first simplification of the model that can be applied within $\Delta\nu$. We emphasize the dependency of κ in this equation (Vilfan et al., 2001):

$$R_1^{OF}(\nu) = A_{OF} \cdot \frac{k_B T}{2\pi\kappa} \sum_{l=2}^{l_{max}} \frac{l(l+1)(2l+1)}{\left(l^2+l-2\right)\left(l^2+l+\sigma\right)} \frac{\tau_l}{\left[1+4\pi^2(\nu+\nu_L)^2\tau_l^2\right]}, \quad (3)$$

where $A_{OF} = (9/8)(1/r)^6\ \gamma^4\hbar^2(\mu_0/4\pi)^2$ with r the mean effective inter-proton distance, γ the proton gyromagnetic ratio, $\hbar$ the Plank's constant divided by 2π and μ_0 the vacuum magnetic permeability; k_B is the Boltzmann constant, T is the temperature, σ is the effective lateral tension, ν_L is the offset field due to the average local field component along the quantization axis and τ_l is given by:

$$\tau_l = \frac{\eta R_0^3}{\kappa} \frac{(2l+1)\left(2l^2+2l-1\right)}{l(l+1)(l+2)(l-1)\left(l^2+l+\sigma\right)}. \quad (4)$$

In the last equation η is the viscosity of the supporting fluid, R_0 the average radius of the spherical liposomes and $l_{max} \approx \pi R_0/d$, where d is the average distance between neighboring molecules. The second term of Eq. (2) associated with diffusion has no direct dependency on κ (Halle, 1991). The fact that κ has a direct influence in the collective motions of the lipids, together with the fact that this is the dominant relaxation mechanism within $\Delta\nu$, suggests that R_1 may be particularly sensitive to the elastic properties of the system within the reduced frequency interval. In the following sections we test this hypothesis.

3. Experimental

3.1. Liposome preparation

Liposomes of lipids suspended in deuterated water were prepared following the procedure already described in Ref. (Fraenza et al., 2014). The average sizes of the unilamellar liposome suspensions were determined using a Nicomp 380 High Performance Particle Sizer (HPPS).

3.2. Relaxation rate dispersion experiments

^{1}H relaxation rate dispersions were measured using two different Spinmaster Fast Field Cycling NMR Relaxometers (Stelar, Mede, Italy). One of them provided with a homogeneous magnetic field (~20 ppm) and magnetic field stability better than 1:10^5. Profiles obtained from this equipment will be called hereafter *measurements in homogeneous magnetic field*. On the other hand, the second apparatus, an older Stelar Spinmaster system had a magnet homogeneity that was degraded to over 350 ppm/cm^3 and field stability lower than 1:10^4. Experiments carried out with this last apparatus will be referred as measurements *in non-homogeneous magnetic field*. Liposome solution samples of 1 cm^3 volume were used. The polarization magnetic field was equivalent to a proton Larmor frequency of 15 MHz and 12 MHz for measurements in homogeneous and non-homogeneous magnetic field, respectively. Polarization pulses of 1 s were used in standard PPS sequences (Anoardo et al., 2001) to measure the magnetization decays. The NMR signal was acquired at a proton Larmor frequency of 14.199 MHz and 9.649 MHz, respectively. A magnetic field slew rate of 3 MHz ms^{-1} was used in all cases, with a switching time of 2 ms. A digitization rate of 1 MHz was used for acquisition, while the signal was acquired 30 μs after the fall-off of the 90° pulse. The FID was sampled with 64 points in the time range 30–94 μs, after the 90° pulse, which was of 6.2 μs length. Each R_1 was determined from a magnetization decay measured with 16 points, each accumulated 12 and 120 times for measurements in homogeneous and non-homogeneous magnetic field, respectively. Sample temperature was controlled to within about 1 K using a Stelar Variable Temperature Controller. Experiments were performed on liposome suspensions with 0, 3, 10 and 20 mol% cholesterol and average hydrodynamic radii of 50 and 54 nm, at different temperatures between 303 and 328 K.

3.3. Modeling the relaxation rate dispersions

For this task we essentially adopted the systematic approach previously discussed (Fraenza et al., 2014; Meledandri et al., 2009; Perlo et al., 2011) with a minor modification. We averaged the

absolute value of deviations between the model curve and the experimental data. We call this quantity *SUM*. The optimal model fitting to the data was obtained by automatically finding the best combination of model parameters that made *SUM* lower than a pre-defined value called SUM_{max} (typically 0.07).

4. Results and data reduction

4.1. Measurements in homogeneous magnetic field

We began this study by validating new measurements in our relaxometer (homogeneous magnetic field, Stelar Spinmaster FC2000/C/D). For this purpose, we reproduced the relaxation rate dispersion of Fig. 1. Experimental data and the model curve corresponding to Eq. (1) can be observed in Appendix A (see Supplementary data). We observed a very good agreement between the experimental data sets and a consistency in the parameters obtained from both model curves.

4.2. Reduced frequency range

In order to test the plausibility to define a universal reduced range $\Delta\nu = \nu_M - \nu_m$ (for liposomes samples), relaxation dispersions were measured for DMPC unilamellar liposomes with cholesterol percentiles of 0mol% and 3mol%, at different temperatures (303 K, 310 K, 318 K and 328 K). The reduced frequency ranges $\Delta\nu$ were calculated for each dispersion profile according to the method described in Section 2. The corresponding values of ν_m and ν_M are summarized in Table 1. It is possible to define an average characteristic reduced frequency range $\Delta\nu_a$, given by $\nu_{ma} = 140 \times 10^3$ Hz and $\nu_{Ma} = 2.5 \times 10^6$ Hz.

4.3. Measurements in non-homogeneous magnetic field

With the purpose of testing the impact of unfavorable experimental conditions on the relaxation rate dispersions, and consequently on the determination of the bending elastic modulus, we ran new measurements at extreme conditions: few data points, non-homogeneous magnetic field, within a restricted frequency range and with a lower magnetic field stability. The error in the measured R_1 reflects the loss of signal-to-noise ratio due to both the lower magnetic field homogeneity and stability. In these experiments we used 54 nm DMPC unilamellar liposomes with different cholesterol percentiles (0%, 3%, 10% and 20%), measured at different temperatures (303 K and 328 K). Measurements were done at six different frequency values: (0.20522, 0.32718, 0.52123, 0.73881, 0.9334, 1.3215) MHz. Fig. 2 shows a typical experiment (DMPC + 3mol% cholesterol at 328 K). The optimal model dispersion (red curve) was obtained using Eq. (2) after finding the optimal values of κ, A_{OF}, D, A_D and R_1^{offset}. Here D represents the diffusion constant and A_D the amplitude of the corresponding spectral density.

Table 1
Reduced frequency ranges $\Delta\nu = \nu_M - \nu_m$ estimated for DMPC liposomes with different molar percentiles of cholesterol and an average radius $R_0 = 50$ nm, measured at 303, 310, 318 and 328 K. We may define a characteristic reduced frequency range from 140×10^3 to 2.5×10^6 Hz.

DMPC			
Cholesterol [%]	T [K] ± 1	ν_m[Hz] × 10^3	ν_M[Hz] × 10^6
0	303	85	1.3
	310	130	1.4
	318	120	2.5
	328	195	5.5
3	328	150	1.8

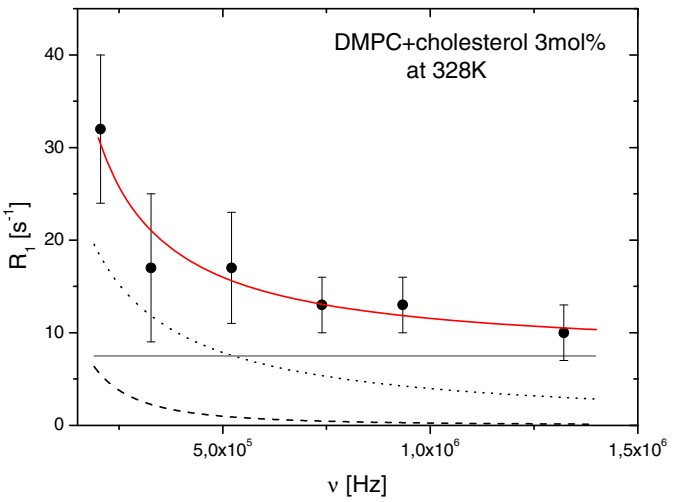

Fig. 2. Relaxation dispersion measured within the restricted frequency range for a DMPC-cholesterol liposome with a percentile of 3 mol% at 328 K. Red solid line: model dispersion, dash line: translational diffusion, dot line: order fluctuations, solid grey line: offset. $\kappa = 2.1 \times 10^{-20}$ J, $A_{OF} = 6.5 \times 10^8 s^{-2}$, $D = 6 \times 10^{-12} m^2 s^{-1}$, $A_D = 10^9 s^{-2}$, $R_1^{offset} = 7 s^{-1}$. Error bars were determined as an interval of 95% of confidence in a *t*-Student distribution of repeated R_1 experiments (10 at each frequency). (For interpretation of the references to color in this figure legend, the reader is referred to the web version of this article.)

A_{OF} and A_D are defined by the mean effective inter-proton distance for each dynamical process, depending much more on the characteristics of the relaxation mechanism itself than the viscoelastic properties of the medium. It is expected only a weak dependence of these amplitudes on the cholesterol content. The considered range in this work goes from $1.6 \times 10^7 s^{-2}$ to $9.9 \times 10^9 s^{-2}$ (Mishra et al., 2006; Perlo, 2011). In contrast, κ and D may depend on the cholesterol content. For the optimization of the model curves, in this work we considered values of κ within the interval 4×10^{-21}–4.2×10^{-19}J and values of D between 10^{-12} and 10^{-10} m^2/s. R_0 (54 nm), d (average distance between neighboring molecules, 1 nm), σ (effective lateral tension, assumed to be negligible) are fixed for all the cases. The viscosity η value was fixed to 1.1×10^{-3}N s/m^2 for $T = 303$ K, and to 0.82×10^{-3}N s/m^2 for $T = 328$ K.

The sensitivity of the simplified model to each parameter was carefully analyzed by considering the response of the theoretical dispersion curve to variations of the parameter value (within a predefined interval that is consistent with the literature). During this process, the rest of the parameters were kept constant. We only considered the model curves that are contained within experimental errors of the data points. From this analysis we can also estimate the corresponding uncertainties for each parameter that is being analyzed (for details see Appendix B (see Supplementary data)). From this study we learn:

1. Order fluctuations are absolutely dominant over diffusion within the restricted frequency range.
2. In an extreme simplification of the model, the diffusion contribution can be neglected within the restricted frequency range. For comparison, we will also evaluate κ under this latter assumption
3. The model is sensitive to the offset, size of the liposomes and local field. This fact suggests that size and local fields (external inputs for the calculations) should conveniently be estimated beforehand.

If we neglect the contribution due to diffusion (extreme simplified model), Eq. (2) simplifies to:

$$R_1(\nu) = R_1^{OF}(\nu) + R_1^{offset} \tag{8}$$

Fig. 3 reproduces the situation of Fig. 2, but now using the extreme simplified model (without the diffusion contribution).

We observe that this new simplification does not affect the obtained value of κ within errors. Parameters corresponding to model dispersions for both cases, Eqs. (2) and (8), for different examined samples and temperatures can be found in the Appendix B (see Supplementary data).

4.4. Effects concerning the homogeneity of the magnetic field

Effects related to a lower homogeneity of the magnetic field on the R_1 Larmor frequency dispersion can be analyzed by considering the extreme simplified model within the restricted frequency interval. It is worth mentioning that the magnetic field inhomogeneity is low enough to ensure that the employed RF pulse still excite all lipid protons within the sample volume, that is, we are not dealing with a strong inhomogeneity situation (Hürlimann, 2007). In the ideal case of extreme homogeneous field, each measured relaxation rate corresponds to a well-defined field (or Larmor frequency) value. In contrast, if a certain degree of magnetic field inhomogeneity is present during the experiment, the measured relaxation rate will have contributions from a frequency interval that is determined by the effective field gradient across the sample. Assuming that the measured effective relaxation rate will be an average within this frequency interval, a possible way of calculation is through the mean value theorem (MVT). It establishes that if a function f is continuous in an interval $[a, b]$, there exists a point c within the interval where the function reaches its mean value, given by (Spivak, 1996):

$$f(c) = \frac{1}{b-a}\int_a^b f(x)dx. \tag{9}$$

When $f(x)$ is linear, the mean value is exactly in the middle of the interval $[a,b]$. An application of MVT to the extreme simplified model (Eq. (8)) gives:

This last equation represents the R_1 value for each frequency interval, due to the presence of a magnetic field inhomogeneity, for a sample whose dispersion in a homogeneous field can be described through Eq. (8). That is, the value we should measure in the presence of the inhomogeneity. In other words, Eq. (10) represents the dispersion we should observe in the inhomogeneous field. This expression may be extended over the whole average dispersion curve $\overline{R}_1(\nu)$ by introducing the field inhomogeneity h in parts per million (ppm):

$$\overline{R}_1(\nu) = A_{OF}\frac{k_B T}{4\pi^2\kappa}\sum_{l=2}^{l_{max}}\frac{l(l+1)(2l+1)}{(l^2+l-2)(l^2+l+\sigma)}\frac{\tan^{-1}\left[2\pi\tau_l\left[2\nu(1+h\cdot 10^{-6})-\nu_L\right]\right]-\tan^{-1}\left[2\pi\tau_l[2\nu(1-h\cdot 10^{-6})-\nu_L)\right]}{2\nu h\cdot 10^{-6}} + R_1^{offset}. \tag{11}$$

In order to analyze the consistency of this result in the practice, we apply Eq. (11) to the data obtained under inhomogeneous field conditions. As the Fourier transform of the free induction decay signal (FID) is still symmetric around the central frequency ν_C, we assume a symmetric contribution of the inhomogeneity at lower and higher frequencies. Therefore, for a 350 *ppm* magnet, we have $h = 175$ *ppm*. Fig. 4 shows $\overline{R}_1(\nu)$ values for DMPC liposomes at 303 K measured in the non-homogeneous magnetic field. The plot also includes the model curve of Eq. (11).

It is worth mentioning that the spread in frequencies generated by the gradient field has a negligible effect on R_1 measurements, which is consistent with the fact that variations of R_1 between the extreme frequencies at each interval are lower than 1%.

5. Discussion

To compare the results using the standard procedure (whole dispersion and using the complete model, i.e., Eq. (1)) with the version here presented (reduced frequency range, magnet homogeneity and lower field stability), relaxation dispersions were measured using the same sample at the same temperature at both experimental conditions. We found an excellent agreement thus validating the proposed methodology and the extreme simplified model. A detailed treatment of the case described in Fig. 4 (DMPC at 303 K) can be found in Appendix C (see Supplementary data).

The values of κ obtained through Eqs. (2) and (8) are consistent. As a consequence of the elimination of the diffusion contribution, the model sensitivity to the value of κ increases. Comparing the values of A_{OF} and R_1^{offset} from both equations, it turns out that using

$$R_1(\nu_C) = A_{OF}\frac{k_B T}{4\pi^2\kappa}\sum_{l=2}^{l_{max}}\frac{l(l+1)(2l+1)}{(l^2+l-2)(l^2+l+\sigma)}\frac{\tan^{-1}[2\pi\tau_l(2\nu_2-\nu_L)]-\tan^{-1}[2\pi\tau_l(2\nu_1-\nu_L)]}{\nu_2-\nu_1} + R_1^{offset}. \tag{10}$$

In this equation ν_C represents the central frequency for each R_1 measurement, while ν_1 and ν_2 are the extreme values of the frequency interval defined by the magnet inhomogeneity (for a given sample length). Since the variations of R_1 are sufficiently smooth within these frequency intervals, we may approach the dispersion by a linear behavior within each interval. As a consequence, we may consider that the mean value is reached at the centre of each interval.

Eq. (8) the order fluctuations contribution increases, while the offset contribution slightly decreases. This is a consequence of the fact that the weak diffusion contribution is now replaced in the extreme simplified model by the other two. In mathematical terms, the functional form of the diffusion term can be replaced in a good approximation by a proper combination of an OF-type function plus a negative offset (see Fig. 2).

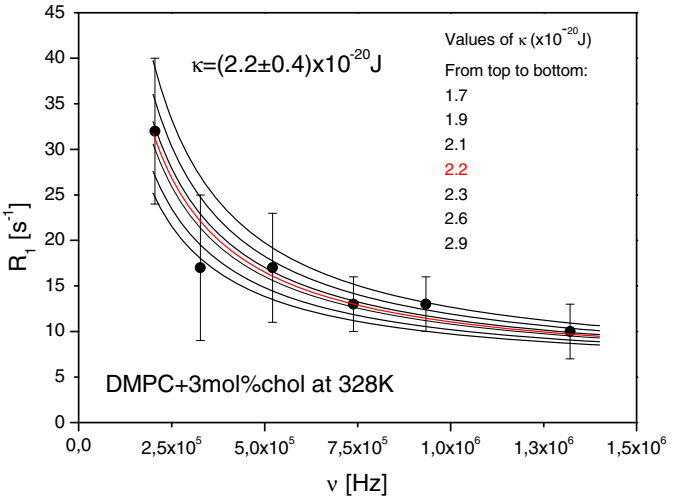

Fig. 3. Relaxation dispersion of Fig. 2 now analyzed using the extreme simplified model, that is, without including the diffusion contribution. Dispersions are shown for different values of κ for fixed values of $A_{OF} = 10 \times 10^8 s^{-2}$ and $R_1^{offset} = 5.5\ s^{-1}$. In red, the new optimal curve obtained from Eq. (8). (For interpretation of the references to color in this figure legend, the reader is referred to the web version of this article.)

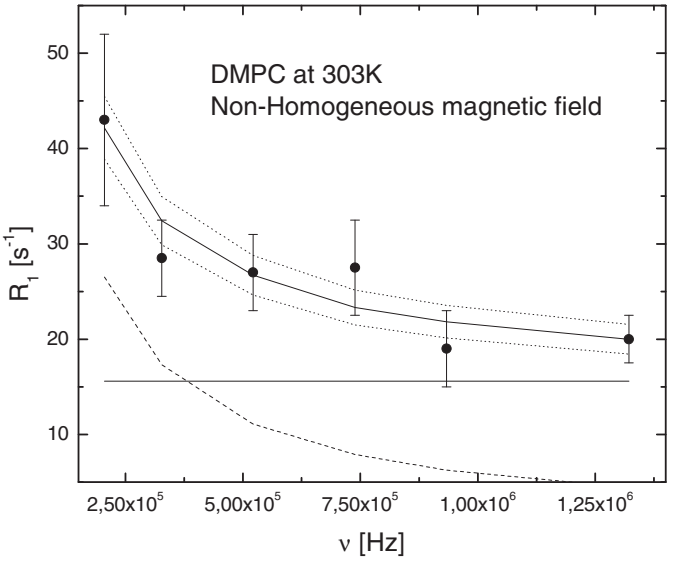

Fig. 4. Average relaxation dispersion measured within the restricted frequency range for DMPC liposomes (average radius $R_0 = 50$ nm), at 303 K using a non-homogeneous magnetic field (●). The MVT model curve of Eq. (11) is shown in black solid line for $\kappa = (2.9 \pm 0.3) \times 10^{-20}$ J, $A_{OF} = (15 \pm 1) \times 10^8\ s^{-2}$ and $R_1^{offset} = (15.6 \pm 0.7)\ s^{-1}$ with $\eta_{D2O} = 0.97 \times 10^{-3}$ kg/s m, $\sigma = 0$ and $a = 1$ nm.

The obtained values for κ are consistent in general with the literature. The tendency to decrease with increasing temperature (Yi et al., 2009; Perlo et al., 2011) can clearly be observed for the 3mol% cholesterol case. The tendency to increase with the cholesterol percentile can also be observed (Méléard et al., 1997; Fraenza et al., 2014). For instance, at $T = 328$ K: $\kappa \sim 2 \times 10^{-20}$ J for 3 mol% cholesterol, while $\kappa \sim 4 \times 10^{-20}$ J for 10 mol% and 20 mol % cholesterol (although we do not see a significant difference between 10 mol% and 20 mol% in these measurements). Nevertheless, the biophysical behavior of DMPC with added cholesterol itself is outside the scope of the present study.

The bending elastic modulus of a lipid bilayer depends on its composition and on the temperature. According to literature, a bilayer made of standard lipids like DMPC, DOPC (1,2-Dioleoyl-sn-glycero-3-phosphocholine) or SPC (soy phosphatidylcholine) has a typical range for the value of this modulus which goes approximately from 8×10^{-21} J for flexible membranes, obtained by addition of detergents, up to 14×10^{-20} J for rigid membranes accomplished by cholesterol addition (Méléard et al., 1997; Pan et al., 2008a, 2008b; Duwe and Sackmann, 1990; Tristram-Nagle et al., 1998; Liu and Nagle, 2004; Mathai et al., 2008; Wachter et al., 2008). This range is fulfilled when the additives reach concentration from 10 to 25mol% and the temperatures are between 288 and 328 K. In this work we obtained for instance a variation of κ by a factor of about 2, with an error of typically 15–30% at T = 328 K, when the cholesterol content increased from 3 to 10/20 mol% (see Table B1, Appendix B (see Supplementary data)). This indicates that the measurement technique, even in the simplified version here presented, is sensitive enough to detect variations in the elastic constant, following the expected tendencies according to the literature.

From Section 4.4 we learn that the effect of the inhomogeneity in the relaxation dispersion (for the current conditions) is negligible. However, a main consequence of the inhomogeneous field in the proposed approach concerns to the associated loss of the signal to noise ratio (SNR) of the NMR signal. This has a direct impact in the number of accumulated signals and the total time of an experiment. However, this point can be partially mitigated using a higher quality reception & detection systems, pulsed shimming coils and other specific hardware, and/or the use of specific NMR pulse sequences (i.e. CPMG, solid echo, etc.).

6. Conclusions

Proton field-cycling NMR relaxometry was used to characterize the lipid dynamics in DMPC membranes with different percetiles of cholesterol. The tendency to a decrease in κ with increasing temperature, and to an increase with the cholesterol percentile was observed, in consistency with a previous study (Fraenza et al., 2014). These results are also consistent with ^{2}H NMR experiments performed in selectively deuterated DMPC (Trouard et al., 1999; Martinez et al., 2002, 2004; Orädd et al., 2009).

We conclude that the field-cycling NMR relaxometry method can be a promising tool for the systematic measurement (in a non-invasive way) of the bending elastic modulus in liposomes and related systems, particularly at sizes that inhibit the applicability of standard optical techniques. According to this study, an instrument operating at moderate homogeneity & stability and within a limited frequency range, offers interesting measurement capabilities, which are consistent with equivalent results obtained in standard state-of-the-art FFC instruments.

It is worth mentioning the relevance of such an instrument for liposome elastometry in view of the continuous development of nanomedical research for drug transportation across the skin through highly deformable vesicles (Dragicevic and Maibach, 2016; Ashtikar et al., 2016), the formulation of other specific liposomes (Silva et al., 2014; Santhosh et al., 2014), testing the stability and rigidity of cross-linkable liposomes (Smith and Kong, 2014), between others. It should be emphasized that in complex samples (for example, model membranes including highly concentrated proteins or other molecules) a clear limitation of this technique originates from the fact that all present protons in the sample contribute to the observed NMR signal. In some cases, it is possible to filter solid-like or liquid-like components by measuring the magnetization evolution at different temporal windows along the FID or other more elaborated suppression techniques. When calamitic molecules (e.g. cholesterol) are added, up to a certain concentration they will be ordered by the lipids and copy the collective dynamics of them (Fraenza et al., 2014).

Determinations of κ in simple formulations have been practiced using a variety of experimental methods: Discrepancies between measurements from different techniques (but similar formulations) can be found in the literature (Bouvaris et al., 2014; Nagle et al., 2015, 2016; Bochiccio and Monticelli, 2016). This feature remains unclear, and the causes of such differences still requires a deeper study. Therefore, it is vital to have access to non-invasive simple techniques, not requiring complicated sample preparation nor complicated theoretical formulations, and with a robust available model for data interpretation. Due to the relevant biophysical significance of a correct characterization of the elastic properties of a biomembrane, the topic deserves more experimental and theoretical effort. The future perspective and potential new applications of FFC for the study of more complex processes involving protein activity or aggregation is promising.

Acknowledgements

This work was supported by funds from Foncyt (PICT-2013-1380), CONICET (PIP6420), Ministerio de Ciencia y Tecnología (Provincia de Córdoba) and Secretaría de Ciencia y Tecnología – Universidad Nacional de Córdoba, Argentina. The authors acknowledge Dr. Guillermo Montich and CIQUIBIC-CONICET for support and access to their laboratories for sample preparation and size evaluation using the HPPS facility.

Appendix A. Supplementary data

Supplementary data associated with this article can be found, in the online version, at http://dx.doi.org/10.1016/j.chemphyslip.2016.10.006.

References

Althoff, G., Stauch, O., Vilfan, M., Frezzato, D., Moro, G., Hauser, P., Schubert, R., Kothe, G., 2002. J. Phys. Chem. B 106, 5517–5526.
Anoardo, E., Galli, G., Ferrante, G., 2001. Appl. Magn. Reson. 20, 365–404.
Armstrong, C.L., Häussler, W., Seydel, T., Katsaras, J., Rheinstädter, M.C., 2014. Soft Matter 10, 2600.
Ashtikar, M., Nagarsekar, K., Fahr, A., 2016. J. Control. Release . http://dx.doi.org/10.1016/j.jconrel.2016.09.008.
Bochiccio, D., Monticelli, L., 2016. Adv. Biomembranes Lipid Self-Assembly 23, 117–143.
Bouvaris, H., Duelund, L., Ipsen, J.H., 2014. Langmuir 30, 13–16.
Brown, M.F., Thurmond, R.L., Dodd, S.W., Otten, D., Beyer, K., 2002. J. Am. Chem. Soc. 124, 8471–8484.
Brown, M.F., 2012. Biochemistry 51, 9782–9795.
Cevc, G., Gebauer, D., 2003. Biophys. J. 84, 1010–1024.
Delmore, N., Fery, A., 2006. Phys. Rev. E 74 030901(R).
Dimova, R., 2014. Adv. Colloid Interface Sci. 208, 225–234.
Dragicevic, N., Maibach, H.I., 2016. Percutaneous penetration enhancers chemical. Methods in Penetration Enhancement. Springer, Berlin.
Duwe, H.P., Sackmann, E., 1990. Physica A 163, 410–428.
Epand, R.M., D'souza, K., Berno, B., Schlame, M., 2015. Biochim. Biophys. Acta 1848, 220–228.
Fraenza, C.C., Meledandri, C., Anoardo, E., Brougham, D., 2014. ChemPhysChem 15, 425–435.
Fujara, F., Kruk, D., Privalov, A.F., 2014. Prog. Nucl. Magn. Resonance Spectrosc. 82, 39–69.
Groves, J.T., 2007. Annu. Rev. Phys. Chem. 58, 697–717.
Hürlimann, M.D., 2007. Magn. Reson. 184, 114–129.
Halle, B., 1991. J. Chem. Phys. 94, 3150–3168.
Henriksen, J., Rowat, A.C., Ipsen, J.H., 2004. Eur. Biophys. 33, 732–741.
Katsaras, J., Guberlet, T., 2000. Lipid Bilayers. Structure and Interaction. Biological Physics Series. Springer, Berlin.
Kimmich, R., Anoardo, E., 2004. Prog. Nucl. Magn. Resonance Spectrosc. 44, 257–320.
Kimmich, R., Schnur, G., Scheuermann, A., 1983. Chem. Phys. Lipids 32, 271–322.
Kinnun, J.J., Mallikarjunaiah, K.J., Petrache, H.I., Brown, M.F., 2015. Biochim. Biophys. Acta 1848, 246–259.
Kotler, S.A., Walsh, P., Brender, J.R., Ramamoorthy, A., 2014. Chem. Soc. Rev. doi: http://dx.doi.org/10.1039/c3cs60431d.
Kruber, S., Farrher, G.D., Anoardo, E., 2013. IEEE Latin Am. Trans. 11, 251–256.
Kruber, S., Farrher, G.D., Anoardo, E., 2014. Can. J. Phys. 92, 1430–1440.
Kruber, S., Farrher, G.D., Anoardo, E., 2015. J. Magn. Reson. 259, 216–224.
Lasalvia, M., Castellani, S., D'Antonio, P., Perna, G., Carbone, A., Colia, A.L., Maffione, A.B., Capozzi, V., Conesse, M., 2016. Exp. Cell Res. (YEXCR10328, in press).
Liu, Y., Nagle, J.F., 2004. Phys Rev E 69, 040901.
Lundbæk, J.A., Collingwood, S.A., Ingólfsson, H.I., Kapoor, R., Andersen, O.S., 2010. J. R. Soc. Interface 7, 373–395.
Méléard, P., Gerbeaud, C., Pott, T., Fernandez-Puente, L., Bivas, I., Mitov, M.D., Dufourc, J., Bothorel, P., 1997. Biophys. J. 72, 2616–2629.
Martinez, G.V., Dykstra, E.M., Lope-Piedrafita, S., Job, C., Brown, M.F., 2002. Phys. Rev. E 66, 050902.
Martinez, G.V., Dykstra, E.M., Lope-Piedrafita, S., Nrown, M.F., 2004. Langmuir 20, 1043–1046.
Mathai, J.C., Tristram-Nagle, S., Nagle, J.F., Zeidel, M.L., 2008. . J. Gen. Physiol. 131, 69–76.
Meledandri, C., Perlo, J., Farrher, E., Brougham, D., Anoardo, E., 2009. J. Phys. Chem. B 113, 15532–15540.
Minetti, C., Vitkova, V., Dubois Bivas, F.I., 2016. J. Phys. Conf. Series 682, 012031.
Mishra, V.K., Anantharamaiah, G.M., Segrest, J.P., Palgunachari, M.N., Chadda, M., 2006. J. Biol. Chem. 281, 6511.
Monzel, C., Sengupta, K., 2016. J. Phys. D 49, 243002.
Mouritsen, O.G., 2004. Lipids 39, 1101–1113.
Nagle, J.F., Jablin, M.S., Tristam-Nagle, S., Akabori, K., 2015. Chem. Phys. Lipids 185, 3–10.
Nagle, J.F., Jablin, M.S., Tristam-Nagle, S., 2016. Chem. Phys. Lipids 196, 76–80.
Nevzorov, A.A., Brown, M.F., 1997. J. Chem. Phys 107, 10288–10310.
Orädd, G., Shahedi, V., Lindblom, G., 2009. Biochim. Biophys. Acta 1788, 1762–1771.
Pan, J., Mills, T.T., Tristam-Nagle, S., Nagle, J.F., 2008a. Phys. Rev. Lett. 100, 198103.
Pan, J., Tristram-Nagle, S., Kučerka, N., Nagle, J.F., 2008b. Biophys. J. 94, 117–124.
Park, Y.K., Best, C.A., Badizadegan, K., Dasari, R.R., Feld, M.S., Kuriabova, T., Henle, M. L., Levine, A.J., Popescu, G., 2010. Proc. Natl. Acad. Sci. U. S. A. 107, 6731–6736.
Perlo, J., Meledandri, C., Anoardo, E., Brougham, D., 2011. J. Phys. Chem. B 115, 3444–3451.
Perlo, J., 2011. PhD Thesis. Universidad Nacional de Córdoba, Argentina.
Pretorius, E., Olumuyiwa-Akeredolu, O., Mbotwe, S., Bester, J., 2016. Blood Rev. 30, 263–274.
Rheinstädter, M.C., Mouritsen, O.G., 2013. Curr. Opin. Colloid Interface Sci. 18, 440–447.
Rommel, E., Noack, F., Meier, P., Kothe, G., 1988. J. Phys. Chem. 92, 2981–2987.
Santhosh, P.B., Velikonja, A., Perutkova, S., Kulkarni, M., Genova, J., Eleršič, K., Iglič, A., Kralj-Iglič, V., Ulrih, N.P., 2014. Chem. Phys. Lipids 178, 52–62.
Silva, J.P.N., Oliveira, A.C.N., Lúcio, M., Gomes, A.C., Coutinho, P.J.G., Oliveira, M.E., 2014. Colloids Surf. B Biointerfaces 121, 371–379.
Smith, C.E., Kong, H., 2014. Langmuir 30, 3697–3704.
Soubias, O., Teague, W.E., Hines, K.G., Mitchell, D.C., Gawrisch, D.C., 2010. Biophys. J. 99, 817–824.
Spivak, M., 1996. Calculus. W.A. Benjamin Inc., New York.
Struppe, J., Noack, F., Klose, G., 1997. Z. Naturforsch 52a, 681–694.
Takechi-Haraya, Y., Sakai-Kato, K., Abe, Y., Kawanishi, T., Okuda, H., Goda, Y., 2016. Langmuir 32, 6074–6082.
Tian, A., Capraro, B.R., Esposito, C., Baumgart, T., 2009. Biophys. J. 97, 1636–1646.
Tomaiuolo, G., 2014. Biomicrofluidics 8, 051501.
Tristram-Nagle, S., Petrache, H.I., Nagle, J.F., 1998. Biophys. J. 75, 917–925.
Trouard, T.P., Nevzorov, A.A., Alam, T.M., Jobb, C., Zajicek, J., Brown, M.F., 1999. J. Chem. Phys. 110, 8802–8818.
Vilfan, V., Althoff, G., Vilfan, I., Kothe, G., 2001. Phys. Rev. E 64, 022902.
Wachter, C., Vierl, U., Cevc, G., 2008. J. Drug Target 16, 611–625.
Yi, Z., Nagao, M., Bossev, D.P., 2009. J. Phys. 21, 155104.
de Meyer, F.J.M., Benjamini, A., Rodgers, J.M., Misteli, Y., Smit, B., 2010. J. Phys. Chem. B 114, 10451–10461.